Optical Depth Measurements of Aerosol, Cloud, and Water Vapor Using Sun Photometers during FIRE Cirrus IFO II

MASATAKA SHIOBARA*

Meteorological Research Institute, Tsukuba, Japan

JAMES D. SPINHIRNE

NASA/Goddard Space Flight Center, Greenbelt, Maryland

AKIHIRO UCHIYAMA AND SHOJI ASANO

Meteorological Research Institute, Tsukuba, Japan

(Manuscript received 17 January 1995, in final form 28 July 1995)

ABSTRACT

Optical depths in the visible to infrared spectral region were obtained from solar extinction measurements with two sun photometers during the First ISCCP Regional Experiment Phase II Cirrus Intensive Field Observation in Kansas.

A method is described to correct sun photometry for gaseous absorption and is extended to estimate the water vapor amount. The approach uses a prior computation of gaseous absorption for the narrowband-pass sun photometry, parameterized with the slant-path absorber amount. These produce correction coefficients for gaseous absorption, as determined by LOWTRAN 7 models. Near-infrared channels were calibrated by modified Langley plots taking account of gaseous absorption.

After the correction and calibration, the aerosol optical depths at the wavelengths of 0.4–4 μm were obtained for clear sky conditions. The aerosol optical depth at the wavelength $\lambda = 0.5$ μm was 0.1–0.2 during the campaign. The cloud optical depth at $\lambda = 0.5$ μm was obtained for cirrus events on 26 November and 5 December 1991 after correction of multiple scattering effects involved in sun photometry. The column amount of water vapor was estimated from the 0.94-μm-channel measurement and compared with results from radiosonde measurements. The comparison has shown a good agreement within a 10% difference during the campaign when the equivalent water vapor amount ranges from 0.3 to 1.2 g cm^{-2}.

1. Introduction

One of the most basic parameters for an atmospheric radiation field study is the optical depth of clouds, aerosols, and absorbing gases. In general, the optical depth in the solar spectral region is obtained from solar extinction measurements with sun photometers. As a contribution to International Satellite Cloud Climatology Project (ISCCP), the First ISCCP Regional Experiment (FIRE) Phase II program conducted the Cirrus Intensive Field Observation (IFO II), 13 November–7 December 1991 in Kansas (McDougal 1993). Various kinds of ground-based radiation instruments participated in the experiment. Spectral solar extinction measurements were performed with sun photometers from the Meteorological Research Institute (MRI) of the Japan Meteorological Agency, the National Aeronautics and Space Administration (NASA), the Pennsylvania State University, and the National Oceanic and Atmospheric Administration. A preliminary comparison of optical depth measurements from the photometers has been presented by Ackerman et al. (1994). In this paper, optical depth analyses from measurements with the MRI and NASA sun photometers are presented and discussed. Results from the optical depth analysis will be an element of the database of the FIRE experiment. Our intent here is to describe the measurements, analysis procedures, and case studies for these results. Some of our results will be compared with other radiation and cloud measurements and theoretical analyses by Kinne et al. (1995, personal communication).

Previously, sun photometers have been widely used for observing the atmospheric turbidity. Studies of at-

* Visiting scientist at NASA/Goddard Space Flight Center in 1991–92 for the research described in this paper.

Corresponding author address: Dr. Masataka Shiobara, Climate Research Dept., Meteorological Research Institute, 1-1 Nagamine, Tsukuba 305, Japan.

mospheric aerosols have used sun photometry to retrieve the size distribution of aerosols by inversion methods applied to the spectral optical depth measurements (e.g., Yamamoto and Tanaka 1969; Shaw et al. 1973; King et al. 1978). Subsequent efforts to expand the wavelength range of measurements to the infrared region were made in order to improve reliability in the retrievals (Spinhirne et al. 1985). In addition to aerosol measurements, sun photometry is also useful for measuring the column amounts of atmospheric minor gases (Volz 1974). Several studies have been made for estimating the column water vapor amount using water vapor absorption at the wavelength $\lambda = 0.94$ μm (e.g., Reagan et al. 1992; Thome et al. 1992; Bruegge et al. 1992a; Faizoun et al. 1994).

Sun photometry is also applicable for estimating cloud optical depth when clouds are thin enough for solar extinction measurements. It should be noted, however, that for clouds a sun photometer measures not only directly attenuated irradiance but also scattered radiance within the field of view (FOV) since cloud particles yield extremely strong forward scattering. For the visible region, Shiobara and Asano (1994) have developed a method to obtain cirrus optical depth by correcting for the multiple scattering involved in sun photometer measurements of ice clouds.

In this paper, a method to correct sun photometry for gaseous absorption at near-infrared (NIR) and infrared (IR) channels is described in detail. The correction is based on transmission calculations with LOWTRAN 7 (Kneizys et al. 1988) and was applied to measurements by a modified Langley calibration method. After the correction and calibration, optical depths in the visible to IR region were successfully obtained. Aerosol optical depth for clear-sky days and cirrus optical depth during the campaign are shown and discussed. The column amount of water vapor was also estimated from sun photometry and compared with results from radiosonde measurements at the same site.

2. Instruments and observation

Two sun photometers acquired spectral solar extinction measurements at several specific wavelengths between 0.4 and 4 μm. A sun photometer from MRI (MRIS), which was manufactured by Eko Instruments Co., Tokyo, model MS-115, was used for measurements in the visible to NIR region. Figure 1 shows a schematic diagram of the MRIS. MRIS includes interference filters with maximum transmission at the wavelengths λ = 368, 421, 502, 676, 864, 938, and 1050 nm, and full widths at half maximum $\Delta\lambda$ = 4–6 nm. A silicon photodiode is used for the detector and controlled to a constant 40°C operating temperature. MRIS was mounted on an equatorial drive to track the sun. Continuous rotation of a filter wheel at the rate of 120 rpm eliminates a zero drift of signal due to the dark photocurrent from the detector. The filter rotation system and the use of sample-and-hold circuits for separating the serial signal allow measurements to be acquired simultaneously for all channels. A more detailed description of the electronics is given in Asano et al. (1995), including a time-sequence chart of the sample-and-hold system. Output signals for all channels were digitized by a data logger, recorded every 10 s temporarily in static memories, and then stored in floppy diskettes through a personal computer.

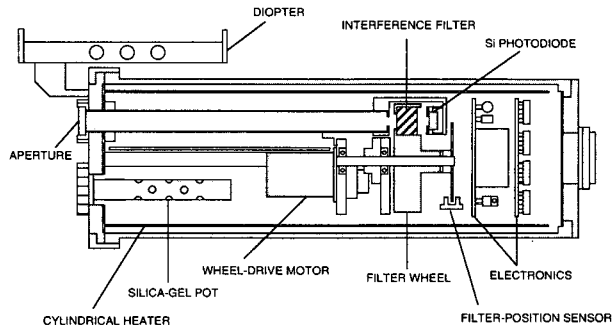

FIG. 1. Schematic diagram of a sun photometer, EKO MS-115, from MRI. The aperture window is made from fused quartz. Eight interference filters are radially installed in the filter wheel. Position of channels is detected by the filter-position sensor using a photointerrupter. The half FOV and slope angles are 1.2° and 0.8°, respectively. The internal dryness is maintained by silica gel in the pot. The internal temperature is controlled at a constant 40°C ± 1°C.

The NASA/Goddard's solar infrared photometer (GSIP) acquired measurements mainly in the NIR to IR region. Details of the GSIP and its performance, along with a functional diagram of the instrument, have been described in Spinhirne et al. (1985). GSIP includes interference filters at λ = 871, 1031, 1225, 1550, 2233, and 3956 nm, with $\Delta\lambda$ = 10–40 nm. A PbSe element is used for the detector and controlled to a constant −10°C operating temperature. GSIP tracks the sun automatically by means of a sun positioning system. Channels are manually selected. Especially for calibration measurements, the channel was switched every 10 s. The signal from GSIP was acquired together with MRIS data.

Both sun photometers were operated side by side at the FIRE site B in the Coffeyville Municipal Airport (37.1°N, 95.6°W, 227 m MSL), Coffeyville, Kansas. At the same site, various radiation instruments were collocated, and simultaneous observations were carried out (Pilewskie and Valero 1993; Ackerman et al. 1994; Kinne et al. 1994). Measurements for clear sky conditions including the data for Langley plot calibrations were made on 9 days with MRIS and GSIP. Cirrus cloud measurements were analyzed for 26 November 1991 with MRIS and GSIP, and for 5 December with MRIS only. Calibration methods for the sun photometers are described below.

3. Correction method for gaseous absorption

When a sun photometer measures the direct solar irradiance for the wavelength λ_0, transmission reduced by gaseous absorption, $T_G(m, \lambda_0)$, along the slant path m is given by the following equation:

$$T_G(m, \lambda_0) = \frac{\int \prod T_i(m, \lambda) f(\lambda) d\lambda}{\int f(\lambda) d\lambda}, \quad (1)$$

where T_i is the transmittance due to each gas absorption and $f(\lambda)$ is the filter function. To have the relationship between the absorber amount and the transmission, that is, a transmittance curve of growth, LOWTRAN 7 (Kneizys et al. 1988) was used for solar transmission calculations to give $T_i(m, \lambda)$ for five atmospheric models for the Tropics, midlatitude summer and winter, and subarctic summer and winter. In this paper, calculations of the solar transmittance were made at eight solar zenith angles, $\theta_s = 0°$, 45°, 60°, 65°, 70°, 73°, 76°, and 78°. The slant-path length is sometimes referred to the optical air mass and is generally given by $m = \sec\theta_s$ for the case where θ_s is not too large to neglect effects of atmospheric refraction. The above eight zenith angles correspond approximately to m = 1, 1.4, 2, 2.4, 2.9, 3.4, 4.1, and 4.8, respectively. In the LOWTRAN model, $T_i(m, \lambda)$ is calculated with respect to the equivalent total absorber amount, which is accumulated along the slant path m taking account of atmospheric refraction.

After calculations of $T_i(m, \lambda)$ by LOWTRAN 7, $T_i(m, \lambda_0)$ was obtained for each channel centered at λ_0 by

$$T_i(m, \lambda_0) = \frac{\int T_i(m, \lambda) f(\lambda) d\lambda}{\int f(\lambda) d\lambda}, \quad (2)$$

where an isosceles triangle with a peak at λ_0 and the bottom length of $2\Delta\lambda$ was assumed for $f(\lambda)$. For more accurate calculations, the real filter response should be used for $f(\lambda)$. Results from calculations assure that $T_i(m, \lambda_0)$ can be simply expressed by the following equation:

$$T_i(m, \lambda_0) = \exp(-k u_i^{\alpha}), \quad (3)$$

where u_i is the equivalent slant-path absorber amount. According to the definition of u_i in the LOWTRAN model, the equivalent column absorber amount x_i is equal to u_i at $\theta_s = 0°$ and is given by the following integral:

$$x_i = \frac{1}{g} \int q_i \left(\frac{p}{p_0}\right)^{\gamma} \left(\frac{T_0}{T}\right)^{\gamma/2} dp, \quad (4)$$

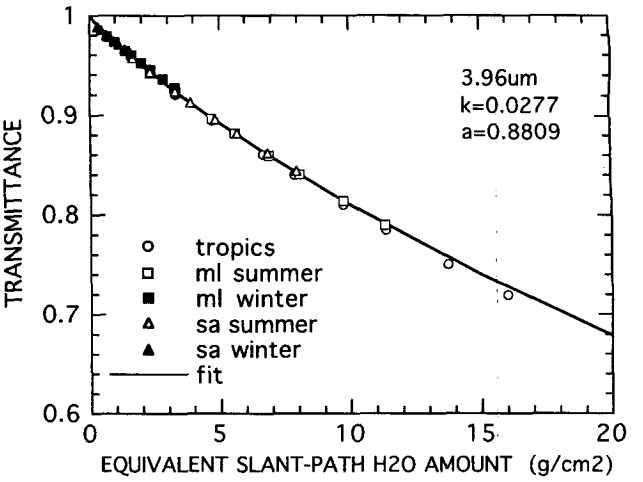

FIG. 2. Solar transmittance at λ = 3.96 μm due to water vapor absorption vs the equivalent slant-path amount of water vapor, calculated by LOWTRAN 7 for tropical (open circles), midlatitude summer (open squares) and winter (solid squares), and subarctic summer (open triangles) and winter (solid triangles) models. The solid curve is a fit to the results using $k = 0.0277$ and $\alpha = 0.8809$ in Eq. (3).

where g is the gravity acceleration, q_i the mass mixing ratio of the absorber, p and T the ambient pressure and temperature, and p_0 and T_0 the standard pressure and temperature, 1013.25 hPa and 273.15 K, respectively. The scaling parameter γ is given to be 0.9 for water vapor. In a strict sense, u_i is different from multiplication of x_i by m. However, it is mostly possible that $u_i = x_i m$ for cases where $\theta_s < 80°$ or $m < 6$. In the following analysis, the equivalent slant-path amount is given by the equivalent column amount x_i multiplied by the optical air mass m.

Figure 2 presents the solar transmittance $T_i(m, \lambda_0)$ due to water vapor absorption at $\lambda_0 = 3.96$ μm. In the figure, symbols denote the values from calculations with LOWTRAN 7 for each model. The least squares fit to all of the plots, as indicated by the solid line, gives $k = 0.0277$ and $\alpha = 0.8809$ in terms of Eq. (3). By the same manner, we have obtained k's and α's for each gas at each channel. In this study, we consider absorption due to water vapor, carbon dioxide, and nitrogen gases at wavelengths longer than 0.9 μm. The results are summarized in Table 1, where x_{H_2O}, x_{CO_2}, and x_{N_2} are defined to be the equivalent column water vapor (g cm^{-2}), CO_2 column amount (atm m), and the atmospheric pressure (atm) at the surface, respectively.

Finally, the transmittance $T_G(m, \lambda_0)$ can be estimated by the following equation:

$$T_G(m, \lambda_0) = \prod T_i(m, \lambda_0). \quad (5)$$

Transmittance is thus parameterized with the equivalent slant-path absorber amount. It must be noted

TABLE 1. Values of k and α in Eq. (3) for the NIR–IR channels, obtained from solar transmittance calculations with the LOWTRAN 7 model; $\Delta\lambda$ is the full width at half maximum of the filter function.

Wavelength (nm)	$\Delta\lambda$	H_2O		CO_2		N_2	
		k	α	k	α	k	α
GSIP							
3956	46	0.0277	0.881	0.0472	0.661	0.559	0.986
2233	24	0.0281	0.840	0.0273	0.581	0	1
1550	10	0.0207	0.856	0.0020	0.612	0	1
1225	10	0.0459	0.691	0.0036	0.703	0	1
1032	10	0.0116	0.882	0.00006	0.710	0	1
MRIS							
1050	4	0.0085	0.973	0.00058	0.701	0	1
938	4	0.6964	0.581	0	1	0	1

that $T_G(m, \lambda_0)$ in Eq. (5) may be different from $T_G(m, \lambda_0)$ in Eq. (1). We have found that both of $T_G(m, \lambda_0)$ mentioned above agree well each other within a 2% difference. Errors involved in parameterization by Eq. (3) and approximation by Eq. (5) are small enough for the correction of gaseous absorption.

4. Modified Langley calibration

A conventional calibration method gives the extraterrestrial output $V_0(\lambda)$, that is, the calibration constant, from the so-called Langley plots. To take account of gaseous absorption, the method should be modified to the following form, using the corrected reading V' in place of the original reading V (Spinhirne et al. 1985):

$$V'(m, \lambda) = \frac{V(m, \lambda)R^2}{T_G(m, \lambda)} = V_0(\lambda) \exp[-\tau(\lambda)m], \quad (6)$$

where R is the sun–earth distance in astronomical units and is omitted in the following equations; $T_G(m, \lambda)$ is calculated by Eqs. (3) and (5) using the gas amount based on observations as described later. The response of the detector is assumed to be constant. Using Eq. (6), the Langley plots are linear, and then the optical depth $\tau(\lambda)$, which excludes any gaseous absorption, can be obtained as well as the zero-airmass intercept $V_0(\lambda)$, that is, the calibration constant. This correction is good for low to moderate absorption. The method is applied for channels longer than 1 μm. An example of a Langley plot for the 3.96-μm channel is shown in Fig. 3. It should be noticed that the Langley plot with uncorrected data leads to a wrong intercept due to the nonlinear effect of gaseous absorption. The difference between the correct and wrong intercepts was 5.5% for this case.

In the Langley plot method, the optical depth is assumed to be constant during the calibration measurement. Unless the change of turbidity is monitored, sun photometry may erroneously determine calibration constants even when the Langley plots are made on a straight line (Shaw 1976; Tanaka et al. 1986). It is very difficult to find a location with good conditions for the Langley calibration. Thus, calibration of sun photometers is still subject to investigation (e.g., Forgan 1994). It is generally acceptable that the calibration error must be small if calibration constants obtained from several independent series of Langley plots agree within a small difference. Results from the Langley calibration for MRIS and GSIP during the campaign are summarized in Table 2. The calibration constant for each channel [$\bar{V}_0(\lambda)$, in Table 2] was determined by averaging three $V_0(\lambda)$ intercepts. The difference among those intercepts for each channel, $\Delta V_0(\lambda)/\bar{V}_0(\lambda)$, except for the 0.94-$\mu$m channel was mostly less than about 2% of the mean value. The uncertainty of 2% of a calibration constant yields an error of 0.01 or less of the optical depth when the optical air mass is 2 or larger.

The water vapor absorption channel, $\lambda = 0.94$ μm, is not well calibrated by the above-mentioned method because the correction of water vapor absorption depends on itself. A further modified method is adopted for the 0.94-μm water vapor channel. Since water vapor absorption is dominant at this channel, the following equation is derived from Eqs. (3) and (6):

$$\frac{V}{T_{R+A}} = V_0 \exp[-k(x_{H_2O}m)^\alpha], \quad (7)$$

where $T_{R+A} = \exp[-(\tau_R + \tau_A)m]$ and τ_R and τ_A are the optical depths for Rayleigh scattering and aerosols, respectively. If τ_A at the water vapor channel can be

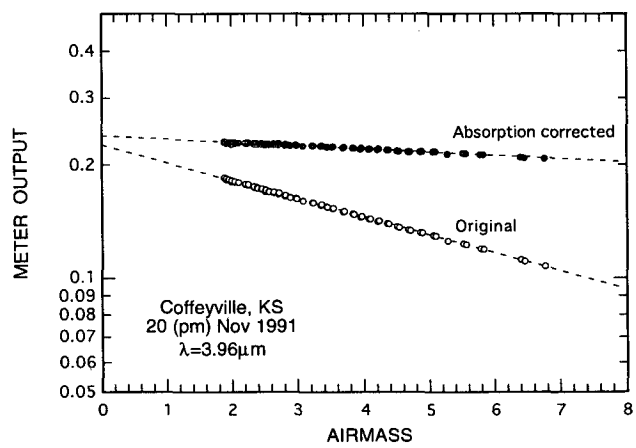

FIG. 3. Langley plots for the 3.96-μm channel, with correction for gaseous absorption effects (upper solid circles) and without correction (lower open circles). The zero-airmass intercept from uncorrected regression is 5.5% smaller than that from the corrected regression.

TABLE 2. Calibration results for MRIS and GSIP from the Kansas experiment: $\bar{V}_0$ is the calibration constant, obtained by averaging three V_0's; τ is the total optical depth excluding water vapor absorption, obtained simultaneously from the Langley calibrations; and ΔV_0 is the difference between the maximum and minimum values of V_0.

GSIP

Wavelength (nm)		871	1032	1225	1550	2233	3956
18 Nov 1991	V_0	1.019	1.090	0.6241	0.5916	0.6723	0.2403
(A.M.)	τ	0.071	0.048	0.041	0.015	0.018	0.019
18 Nov 1991	V_0	1.033	1.146	0.6418	0.6016	0.6883	0.2440
(P.M.)	τ	0.074	0.050	0.047	0.021	0.024	0.020
20 Nov 1991	V_0	1.019	1.098	0.6288	0.5937	0.6736	0.2390
(P.M.)	τ	0.073	0.054	0.043	0.020	0.020	0.018
Mean	$\bar{V}_0$	1.024	1.111	0.6316	0.5956	0.6781	0.2411
$\Delta V_0/\bar{V}_0$		0.014	0.050	0.028	0.017	0.024	0.021

MRIS

Wavelength (nm)		368	421	502	676	864	938	1050
18 Nov 1991	V_0	6.095	10.55	6.688	6.977	3.099	17.67	2.304
(A.M.)	τ	0.597	0.374	0.231	0.116	0.073		0.051
18 Nov 1991	V_0	6.024	10.61	6.793	7.095	3.116	21.32	2.338
(P.M.)	τ	0.595	0.382	0.238	0.124	0.076		0.055
20 Nov 1991	V_0	5.971	10.28	6.648	6.944	3.095	20.56	2.315
(P.M.)	τ	0.603	0.383	0.238	0.123	0.077		0.057
Mean	$\bar{V}_0$	6.030	10.48	6.710	7.005	3.103	19.85	2.319
$\Delta V_0/\bar{V}_0$		0.021	0.031	0.022	0.022	0.007	0.18	0.015

obtained from interpolation between neighboring channels, that is, $\lambda = 0.86$ and 1.05 μm in this study, T_{R+A} comes to be a known value. Then a new plot is possible where the abscissa is m^α in place of conventional air mass m (Bruegge et al. 1992a). This study employs $\alpha = 0.581$ as given in Table 1. For the same channel, Bruegge et al. (1992a) have obtained $\alpha = 0.57$ from a similar procedure using LOWTRAN 7. Several previous studies have employed $\alpha = 0.5$ on the basis of the square-root assumption for water vapor absorption (e.g., Reagan et al. 1992; Thome et al. 1992; Faizoun et al. 1994). Figure 4 shows such plots for the 0.94-μm channel. A calibration constant was thus obtained. The convergence of intercepts during the campaign was several times worse than that for other channels as shown in Table 2. Accurate determination of the calibration constant needs a stable condition of water vapor amount during the calibration measurement just as the usual Langley plot calibration needs a stable turbidity condition. The result might be affected by the diurnal change of water vapor amount.

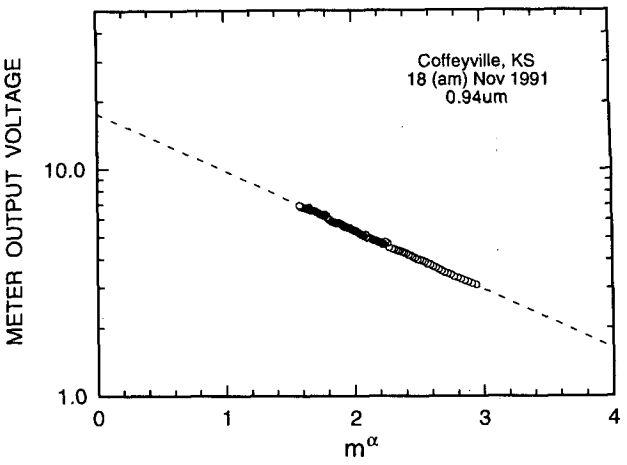

FIG. 4. A modified Langley plot for the 0.94-μm water vapor channel, employing the abscissa of m^α ($\alpha = 0.581$) in place of the conventional air mass m.

5. Observational results and discussion

a. *Aerosol optical depths*

The aerosol optical depth τ_A is obtained by subtraction of optical depths due to Rayleigh scattering τ_R and gaseous absorption τ_G from the total optical depth τ_T, that is, $\tau_A = \tau_T - \tau_R - \tau_G$. We adopt Fröhlich and Shaw (1980) for calculating τ_R but with a 3.1% increased factor according to the suggestion by Young (1980). Absorption by ozone is considered in τ_G at channels in the Chappuis band. In this study, τ_G for the 0.5- and 0.68-μm channels are given to be constant 0.008 and 0.012, respectively. For $\lambda > 1$ μm, absorption by water vapor, CO_2, and N_2 is taken into account as described in the previous section. The equivalent column water vapor is estimated by the integral of Eq. (4) using the vertical profile of relative humidity mea-

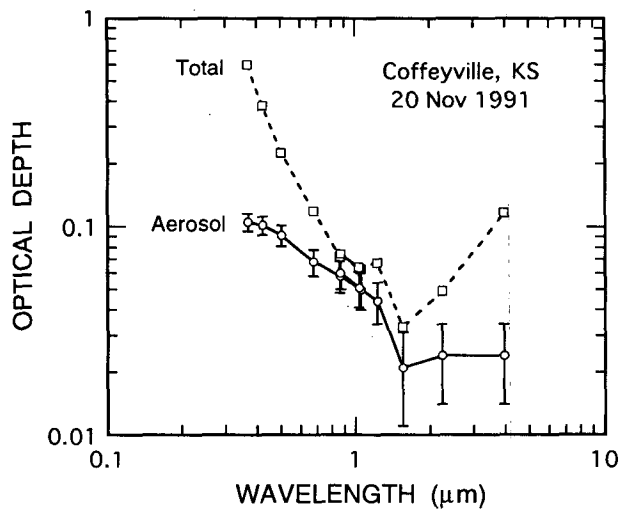

FIG. 5. Total (squares) and aerosol (circles) optical depths measured by MRIS (for wavelengths $\lambda < 1$ μm) and GSIP (for wavelengths $\lambda > 0.8$ μm). Daily average values are plotted for the 20 November case. Error bars indicate the ± 0.01 uncertainty of the aerosol optical depth.

sured by the CLASS (Cross-chain Loran Atmospheric Sounding System) radiosondes that were launched at the same site. For CO_2 amount, the midlatitude winter model in LOWTRAN 7 is adopted. As mentioned earlier, N_2 absorption is parameterized in terms of the atmospheric pressure x_{N_2} (atm).

The aerosol optical depths in the visible to IR (0.4–4 μm) region were analyzed for 9 days under clear sky conditions during the experiment. Daily mean values of the aerosol optical depths thus obtained from MRIS and GSIP are summarized in Table 3. The change in aerosol optical depth $\Delta\tau_A$ is the rms deviation of the aerosol optical depth from the daily mean value $\bar{\tau}_A$. There were no observations with GSIP on 23–24 November or 3–5 December 1991.

Figure 5 shows the total and aerosol optical depths at 13 channels measured on 20 November 1991. Looking at the overlapping channels, $\lambda = 0.86$ and 0.87 μm and $\lambda = 1.05$ and 1.03 μm, the optical depths from MRIS and GSIP agree well, and measurements have been made with sufficient accuracy. Results are dependent on the wavelength transmission characteristics of filters installed in sun photometers. The response curves have been measured with spectrophotometers at MRI and NASA/Goddard Space Flight Center. There were no significant errors in the response curve of filters. As shown in Fig. 5, the optical depth due to gaseous absorption accounts for a large portion of the total optical depth for channels larger than 1 μm, where the Rayleigh optical depth is small. Thus, a small uncertainty in the estimation of water vapor absorption can significantly affect the estimation of the aerosol optical depth. For the 1.55-μm channel, the result shows possibly an excessive water vapor absorption. On the other hand, gaseous absorption for the 3.96-μm channel might be underestimated. It should be noticed, however, that the 0.01 uncertainty is not eliminated from the optical depth obtained in the present analyses as discussed earlier. For reference, each error bar in the figure shows a ± 0.01 uncertainty of the optical depth. Similar to our result, Spinhirne (1994) has reported a disagreement in the airborne

TABLE 3. Daily mean values $\bar{\tau}_A$ and the rms deviations $\Delta\tau_A$ of the aerosol optical depth during the 1991 FIRE Cirrus IFO II, Coffeyville, Kansas. They are estimated by averaging daily data for the period from the time "start LST" through the time "end LST" in the bottom lines. Cloudy data have been eliminated from the statistics.

λ (nm)		18 Nov	20 Nov	21 Nov	23 Nov	24 Nov	26 Nov	3 Dec	4 Dec	5 Dec
368	$\bar{\tau}_A$	0.096	0.105	0.100	0.205	0.165	0.200	0.185	0.141	0.133
	$\Delta\tau_A$	0.009	0.007	0.006	0.009	0.025	0.011	0.029	0.009	0.014
421	$\bar{\tau}_A$	0.087	0.101	0.098	0.194	0.157	0.176	0.163	0.124	0.120
	$\Delta\tau_A$	0.008	0.005	0.007	0.005	0.026	0.010	0.027	0.006	0.012
502	$\bar{\tau}_A$	0.082	0.091	0.087	0.183	0.143	0.152	0.155	0.113	0.113
	$\Delta\tau_A$	0.005	0.003	0.005	0.004	0.027	0.006	0.025	0.006	0.012
676	$\bar{\tau}_A$	0.058	0.068	0.069	0.143	0.118	0.110	0.121	0.081	0.087
	$\Delta\tau_A$	0.004	0.002	0.005	0.004	0.028	0.005	0.021	0.006	0.013
864	$\bar{\tau}_A$	0.050	0.058	0.065	0.123	0.100	0.104	0.127	0.092	0.093
	$\Delta\tau_A$	0.003	0.002	0.006	0.011	0.029	0.011	0.023	0.012	0.020
871	$\bar{\tau}_A$	0.058	0.060	0.068	—	—	0.096	—	—	—
	$\Delta\tau_A$	0.003	0.002	0.005						
1032	$\bar{\tau}_A$	0.046	0.051	0.059	—	—	0.084	—	—	—
	$\Delta\tau_A$	0.003	0.002	0.007						
1050	$\bar{\tau}_A$	0.047	0.050	0.055	0.090	0.085	0.075	0.084	0.058	0.068
	$\Delta\tau_A$	0.003	0.002	0.004	0.007	0.032	0.005	0.014	0.005	0.016
1225	$\bar{\tau}_A$	0.043	0.044	0.055	—	—	0.078	—	—	—
	$\Delta\tau_A$	0.003	0.002	0.006						
1550	$\bar{\tau}_A$	0.018	0.021	0.028	—	—	0.041	—	—	—
	$\Delta\tau_A$	0.002	0.001	0.006						
2233	$\bar{\tau}_A$	0.023	0.024	0.031	—	—	0.038	—	—	—
	$\Delta\tau_A$	0.002	0.002	0.006			0.006			
3956	$\bar{\tau}_A$	0.021	0.024	0.030	—	—	0.045	—	—	—
	$\Delta\tau_A$	0.002	0.002	0.003						
Start LST		0737	1204	0749	0805	1419	0755	0922	0754	0755
End LST		1557	1614	1609	1204	1633	1100	1630	1618	1000

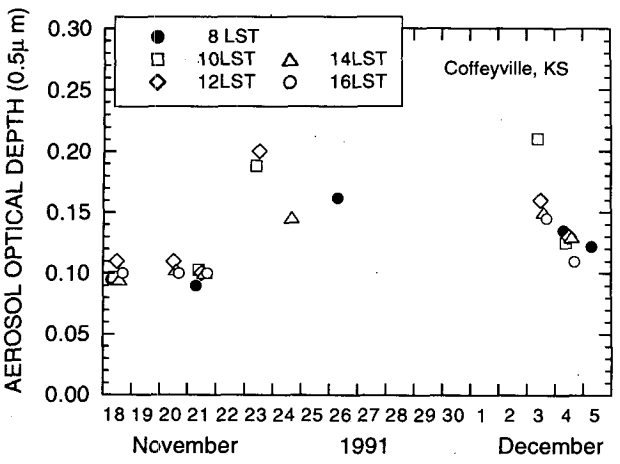

FIG. 6. Temporal change of aerosol optical depth at $\lambda = 0.5$ μm during the Kansas campaign. Average values for 10 min around 0800, 1000, 1200, 1400, and 1600 LST are denoted by solid circles, squares, diamonds, triangles, and open circles, respectively.

GSIP-observed and LOWTRAN 7–calculated water vapor optical depths at $\lambda = 1.55$ and 2.23 μm. Measurements with higher accuracy are necessary for further quantitative discussion. Such measurements may contribute to answer the uncertainty of water vapor absorption in NIR region.

The aerosol optical depth at $\lambda = 0.5$ μm was about 0.1–0.2 during the campaign as shown in Fig. 6. The result is similar to those from Bruegge et al. (1992b), who have measured the aerosol optical depth with sun photometers in the Konza Prairie, Kansas, and reported that the aerosol optical depth for the midvisible region around $\lambda = 0.5$ μm was 0.05–0.2 over the Konza. Simultaneous Lidar observations in the FIRE site have detected the enhancement of the stratospheric aerosols due to the June 1991 eruption of Mount Pinatubo in the Philippines (Sassen et al. 1995). It is expected that the aerosol optical depth obtained here includes some portion of the optical depth of the enhanced stratospheric aerosols. However, it is difficult to extract the effect of the Pinatubo eruption on the optical depth from ground-based passive measurements.

b. Cirrus optical depth at $\lambda = 0.5$ μm

Sun photometers measure not only the directly attenuated solar irradiance but also a radiance scattered into the instrument's aperture since any instrument has a finite FOV. In particular, the scattering by ice clouds may not be ignored. Multiple scattering into the FOV causes an excessive transmission, and thus the optical depth may be apparently underestimated. To accurately obtain the cirrus optical depth, it is important to correct for multiple scattering by ice crystals in the clouds. Our measurements for cirrus clouds were corrected by a method developed by Shiobara and Asano (1994). The method is based on the Monte Carlo radiative transfer simulations for multiple scattering in ice clouds. The correction method uses the following relationship between the true optical depth τ and the apparent optical depth due to multiple scattering τ^*:

$$\tau = \frac{\tau^*}{1 - \omega P \Delta\Omega}, \tag{8}$$

where the term $\omega P \Delta\Omega$ means the portion of forward scattering within the FOV. The MRIS has a full FOV angle of 2.4°, and $\omega P \Delta\Omega$ is given to be 0.49 when a phase function for ice clouds calculated by Takano and

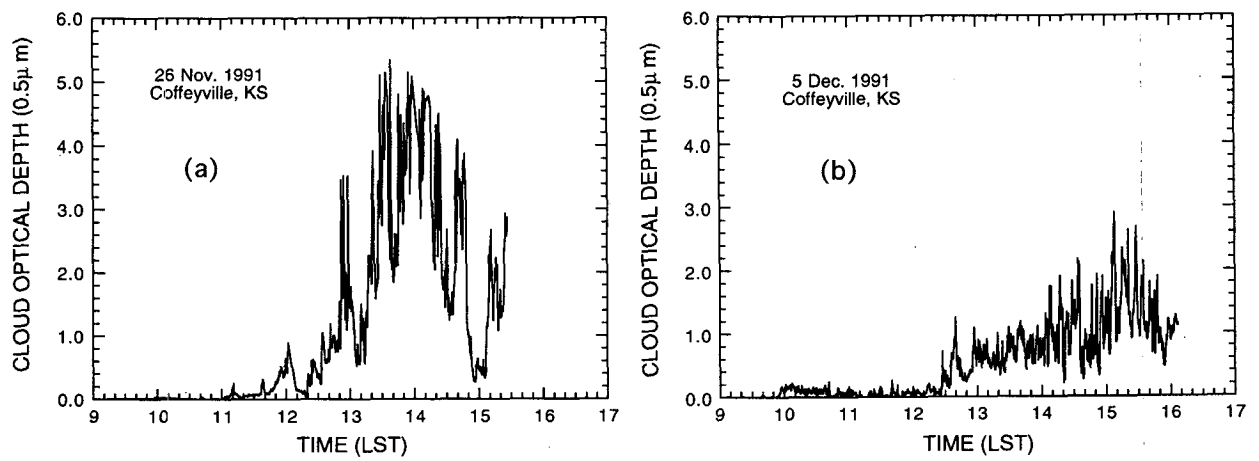

FIG. 7. Time series of cloud optical depth at $\lambda = 0.5$ μm observed on (a) 26 November 1991 and (b) 5 December 1991 under cirrus conditions. The aerosol optical depth was assumed to be a constant value of 0.16 and 0.12 during the day of 26 November and 5 December, respectively.

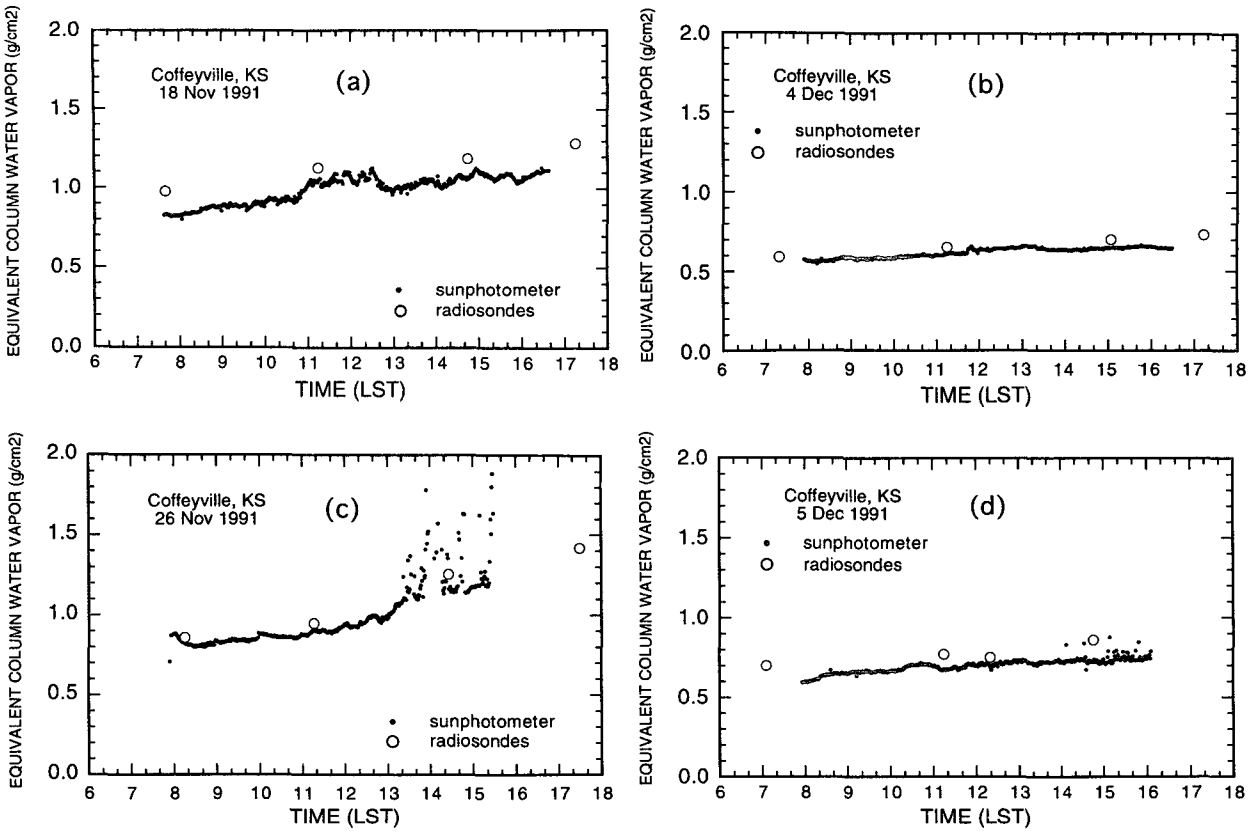

FIG. 8. Time series of the equivalent column water retrieval from sun photometry (closed circles) in comparison with CLASS measurements (open circles) for clear-sky cases on (a) 18 November and (b) 4 December 1991, and for cirrus events on (c) 26 November and (d) 5 December 1991.

Liou (1989) is used in the correction (Shiobara and Asano 1994).

Figure 7 shows time variations of cloud optical depth at $\lambda = 0.5$ μm for cirrus conditions observed on 26 November and 5 December 1991. We could observe halos from ice crystals around noon of 26 November. The cloud then became thick and was possibly accompanied by lower clouds such as altocumulus in the afternoon. For the 5 December case, the cloud was not excessively thick, and the optical depth did not vary widely from a value of one. The cloud optical depth excludes optical depth due to aerosols. The aerosol optical depths have been estimated to be 0.16 and 0.12 for 26 November and 5 December, respectively, from observations under visually cloud-free conditions before 1000 LST of both days. It is expected, however, that there might be some diurnal change of the aerosol optical depth for those days. The assumption of constant aerosol optical depth causes an error in the cloud optical depth. The uncertainty for the 0.5-μm channel is roughly expected to be ± 0.02 from variations shown in Table 3 and Fig. 6.

Measurements were not effective for $m\tau^* > 5$, or $m\tau > 10$, because of limitation of the signal-to-noise performance of MRIS. Therefore the cloud optical depth is not plotted in the region where $m\tau > 10$ in Fig. 7. For example, there are no values of cloud optical depth over 5 on 26 November, although the cloud optical depth exceeded 5 frequently around 1400 LST. All data are shown for the 5 December case since the cirrus clouds were consistently thin. It is suggested that sun photometry is useful for optical depth measurements of cirrus clouds when $m\tau$ is less than 10.

The correction method employed the scattering phase function for a cirrostratus model described in Takano and Liou (1989) and was applied to measurements at $\lambda = 0.5$ μm only. The correction factor $\beta = (1 - \omega P \Delta\Omega)^{-1}$ is 1.96 in this study. The correction factor depends on the forward part of the phase function, which is sensitive to the shape and size of ice crystals. Estimations by Kinne et al. (1995, personal communication) have shown that the values of $\beta = 1.8$–2.5 are expected for various ice cloud models given in Takano and Liou (1989). The result

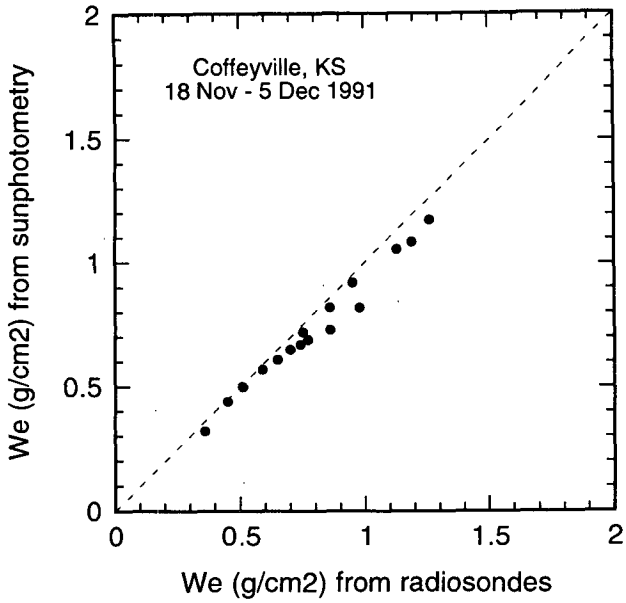

FIG. 9. A comparison of the equivalent column water vapor amount from sun photometer (ordinate) and CLASS (abscissa) measurements for common times during the experiment. The least squares fit to the data yields a linear regression curve $y = ax$ with $a = 0.93$ (±0.02, 95% reliability).

in this paper may be improved by using phase functions based on observations for cirrus clouds during the campaign when these are available.

c. Column water vapor retrievals

Measurements at the 0.94-μm channel enable estimates of the column amount of water vapor. According to Eq. (7), the equivalent column amount x_{H_2O} can be obtained from the following equation:

$$x_{H_2O} = \frac{1}{m}\left[-\frac{1}{k}\ln\left(\frac{1}{V_0}\frac{V}{T_{R+A}}\right)\right]^{1/\alpha}. \qquad (9)$$

Figure 8 shows temporal variation of the column water vapor for the clear-sky cases [(a) and (b)] and the cloudy cases [(c) and (d)]. Solid circles are calculated from Eq. (9) using sun photometer data. For comparisons, open circles are calculated from Eq. (4) using the humidity profile measured by CLASS. It is evident that the scatter of solid circles at 1330–1530 LST 26 November and around 1500 LST 5 December in Fig. 8 is not true and is possibly affected by clouds. As a result, it is found that the water vapor retrieval from sun photometer measurements is effective even for the cloudy condition when the optical depth is less than 1. Comparisons between CLASS soundings and sun photometer measurements during the campaign are summarized in Fig. 9. The water vapor amount from sun photometry is estimated slightly smaller than that from radiosondes but agrees well within a 10% difference where the equivalent water vapor ranges from 0.3 to 1.2 g cm^{-2}. It is generally known that accurate measurement of humidity from radiosondes is very difficult and the uncertainty increases in low-humidity conditions. Reagan et al. (1995) have compared the column water vapor retrievals from sun photometry with those from not only radiosondes but also microwave radiometer measurements. They have found a good coincidence among those measurements within 0.1 cm of the precipitable water vapor amount and a percent difference generally within 10%. Our result is comparable to those from Reagan et al. (1995) and Thome et al. (1992).

In this study, the measurement at the water vapor channel is related to the *equivalent* column water vapor amount. We sometimes use an amount of the *precipitable* water vapor, which is an important parameter for precipitation and water budget. The precipitable amount is a vertically accumulated water vapor amount as defined by Eq. (4) but with $\gamma = 0$. It is evident that the values of these two quantities are different from each other. Furthermore, even for cases where the precipitable water vapor amounts are equal, the equivalent water vapor amount may possibly yield different values depending on vertical profiles. However, a good correlation is still expected between the equivalent column water vapor w_e and the precipitable water vapor w_p as shown in Fig. 10. For the Kansas experiment, the following relationship has been found:

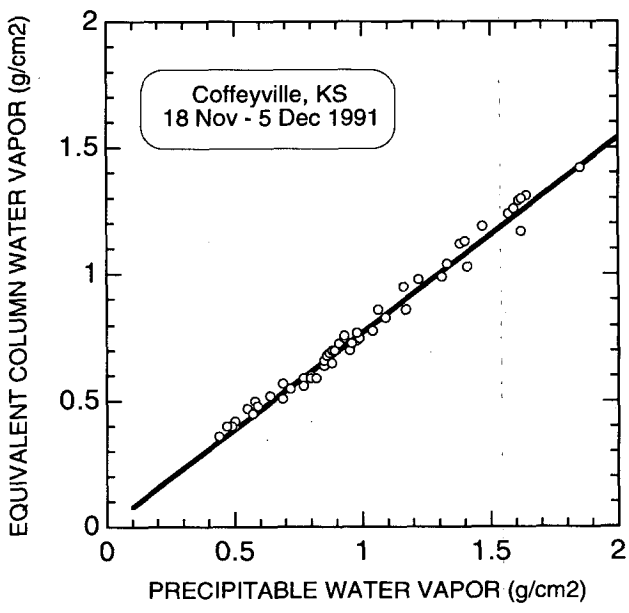

FIG. 10. The relationship between the precipitable water vapor and the equivalent column water vapor estimated from humidity profiles by CLASS soundings. A linear regression curve given by Eq. (10) is drawn by the solid line.

$$w_p = 1.29 w_e \pm \epsilon, \quad (10)$$

where $\epsilon = 0.03$ (g cm^{-2}) for this case is the rms deviation of data from a linear regression curve. The relationship may vary from season to season or place to place since it depends on the vertical profile of water vapor. If the relationship is statistically effective, it is possible to estimate the precipitable water vapor amount from the equivalent column amount obtained from sun photometer measurements using Eq. (9).

6. Summary

During the FIRE Cirrus IFO II in Kansas, we performed spectral solar extinction measurements at the wavelengths between 0.4 and 4 μm using two sun photometers from MRI and NASA. The optical depth measurements will be part of the database of observations from the experiment. The measurements and analysis procedures are documented in this paper.

We first investigated the gaseous absorption at the sun photometer channels in NIR to IR by transmission calculations using LOWTRAN 7 models. Those calculations derived absorption parameters k and α as defined by Eq. (3), which characterize gaseous absorption for H_2O, CO_2, and N_2 at the given channels. Corrections using k and α, which are summarized in Table 1, should exclude uninvited effects due to gaseous absorption on calibration and aerosol optical depth analyses for the NIR–IR channels. For the water vapor channel $\lambda = 0.94$ μm, a modified Langley plot method adopted m^α for the scale of the abscissa in place of the conventional air mass m (Fig. 4).

We successfully obtained the aerosol optical depths after correction for gaseous absorption. The aerosol optical depth at $\lambda = 0.5$ μm was 0.1–0.2 during the Kansas campaign (Fig. 6). The result from NIR measurements suggests possibly an excessive water vapor absorption amount calculated for the 1.55-μm channel.

The optical depth for cirrus clouds at $\lambda = 0.5$ μm was measured on 22 November and 5 December 1991 (Fig. 7). It is suggested that sun photometry is useful for optical depth measurements of cirrus clouds when $m\tau$ is less than 10. Even though good results were obtained, the multiple scattering correction applied in this study may be further improved when a phase function based on in situ measurements is available.

The equivalent column water vapor was retrieved from measurements at the 0.94-μm channel (Fig. 8). The measurement was valid for cloudy cases where the cloud optical depth was less than 1. The comparison between results from sun photometry and radiosonde measurements has shown a good agreement within a 10% difference during the campaign when the equivalent water vapor amount ranges from 0.3 to 1.2 g cm^{-2}.

Acknowledgments. When this work was done, M. Shiobara was a National Research Council Research Associate at NASA/Goddard Space Flight Center on leave from MRI, Japan. Participation of A. Uchiyama in the campaign was supported by the Science and Technology Agency of the Japanese Government as part of the Japanese Cloud-Climate Study (JACCS) Program. The authors sincerely thank the FIRE Project staff, especially Dr. J. Suttles and Mr. D. McDougal, for providing the opportunity to participate in the experiment and supporting this study. Dr. T. Ackerman helped to successfully carry out our observations at the campaign site. Atmospheric profile data from CLASS for the water vapor analysis were courtesy of Drs. D. Starr and J. Titlow. Transmission calculations using LOWTRAN 7 were provided by Mr. W. Hart. An initial suggestion by Prof. M. Tanaka and discussion with Dr. K. Thome were useful for water vapor retrievals in this study. Helpful comments and suggestions by an anonymous reviewer should also be acknowledged for improving the paper.

REFERENCES

Ackerman, T. P., J. A. Valero, S. Kinne, P. Pilewskie, F. P. J. Valero, S. A. Ackerman, and M. Shiobara, 1994: A comparison of cirrus cloud optical depths determined from ground-based, passive radiation measurements during FIRE Cirrus II. Preprints, *Eighth Conf. on Atmospheric Radiation,* Nashville, TN, Amer. Meteor. Soc., 220–224.

Asano, S., M. Shiobara, Y. Nakanishi, and Y. Miyake, 1995: A multichannel cloud pyranometer system for airborne measurement of solar spectral reflectance by clouds. *J. Atmos. Oceanic Technol.,* **12,** 479–487.

Bruegge, C. J., J. E. Conel, R. O. Green, J. S. Margolis, R. G. Holm, and G. Toon, 1992a: Water vapor column abundance retrievals during FIFE. *J. Geophys. Res.,* **97,** 18 759–18 768.

——, R. N. Halthore, B. M. Markham, M. Spanner, and R. Wrigley, 1992b: Aerosol optical depth retrievals over the Konza Prairie. *J. Geophys. Res.,* **97,** 18 743–18 758.

Faizoun, C. A., A. Podaire, and G. Dedieu, 1994: Monitoring of Sahelian aerosol and atmospheric water vapor content characteristics from sun photometer measurements. *J. Appl. Meteor.,* **33,** 1291–1303.

Forgan, B. W., 1994: General method for calibrating sun photometers. *Appl. Opt.,* **33,** 4841–4850.

Fröhlich, C., and G. E. Shaw, 1980: New determination of Rayleigh scattering in the terrestrial atmosphere. *Appl. Opt.,* **19,** 1773–1775.

King, M. D., D. M. Byrne, B. M. Herman, and J. A. Reagan, 1978: Aerosol size distributions obtained by inversion of spectral optical depth measurements. *J. Atmos. Sci.,* **35,** 2153–2167.

Kinne, S., R. Bergstrom, T. P. Ackerman, A. J. Heymsfield, J. DeLuisi, M. Shiobara, P. Pilewskie, F. P. J. Valero, and Y. Takano, 1994: Cirrus cloud solar radiative properties: Comparisons between theory and observations based measurements during FIRE'91. Preprints, *Eighth Conf. on Atmospheric Radiation,* Nashville, TN, Amer. Meteor. Soc., 238–240.

Kneizys, F. X., E. P. Shettle, L. W. Abreu, J. H. Chetwynd, G. P. Anderson, W. O. Gallery, J. E. A. Selby, and S. A. Clough, 1988: Users guide to LOWTRAN 7. AFGL-TR-88-0177, 137 pp.

McDougal, D., 1993: *FIRE Cirrus Science Results 1993.* NASA Conference Publ. 3238, 214 pp.

Pilewskie, P., and F. P. J. Valero, 1993: Ground-based passive remote sensing during FIRE IFO II. *FIRE Cirrus Science Results 1993,* NASA CP 3238, 115–116.

Reagan, J., K. Thome, and B. Herman, 1992: A simple instrument and technique for measuring columnar water vapor via near-IR differential solar transmission measurements. *IEEE Trans. Geosci. Remote Sens.*, **30,** 825–831.

——, ——, ——, R. Stone, J. DeLuisi, and J. Snider, 1995: A comparison of columnar water vapor retrievals obtained with near-IR solar radiometer and microwave radiometer measurements. *J. Appl. Meteor.*, **34,** 1384–1391.

Sassen, K., D. O'C. Starr, G. G. Mace, M. R. Poellot, S. H. Melfi, W. L. Eberhard, J. D. Spinhirne, E. W. Eloranta, D. E. Hagen, and J. Hallett, 1995: The 5–6 December 1991 FIRE IFO II jet stream cirrus case study: Possible influences of volcanic aerosols. *J. Atmos. Sci.*, **52,** 97–123.

Shaw, G. E., 1976: Error analysis of multi-wavelength sun photometry. *Pure Appl. Geophys.*, **114,** 1–14.

——, J. A. Reagan, and B. M. Herman, 1973: Investigations of atmospheric extinction using direct solar radiation measurements made with a multiple wavelength radiometer. *J. Appl. Meteor.*, **12,** 347–380.

Shiobara, M., and S. Asano, 1994: Estimation of cirrus optical thickness from sun photometer measurements. *J. Appl. Meteor.*, **33,** 672–681.

Spinhirne, J. D., 1994: Comparison of measured and calculated water vapor absorption in the near infrared. Preprints, *Eighth Conf. on Atmospheric Radiation,* Nashville, TN, Amer. Meteor. Soc., 164–165.

——, M. G. Strange, and L. R. Blaine, 1985: Solar infrared photometer. *J. Atmos. Oceanic Technol.*, **2,** 264–267.

Takano, Y., and K.-N. Liou, 1989: Solar radiative transfer in cirrus clouds. Part I: Single-scattering and optical properties of hexagonal ice crystals. *J. Atmos. Sci.*, **46,** 3–19.

Tanaka, M., T. Nakajima, and M. Shiobara, 1986: Calibration of a sun photometer by simultaneous measurements of direct-solar and circumsolar radiations. *Appl. Opt.*, **25,** 1170–1176.

Thome, K. J., B. M. Herman, and J. A. Reagan, 1992: Determination of precipitable water from solar transmission. *J. Appl. Meteor.*, **31,** 157–165.

Volz, F. E., 1974: Economical multispectral sun photometer for measurements of aerosol extinction from 0.44 micron to 1.6 micron and precipitable water. *Appl. Opt.*, **13,** 1732–1733.

Yamamoto, G., and M. Tanaka, 1969: Determination of aerosol size distribution from spectral attenuation measurements. *Appl. Opt.*, **8,** 447–453.

Young, A. T., 1980: Revised depolarization corrections for atmospheric extinction. *Appl. Opt.*, **19,** 3427–3428.